JOURNAL OF MATERIALS SCIENCE 12 (1977) 1071–1087

Review
Electron channelling patterns in scanning electron microscopy

E. M. SCHULSON
Materials Science Branch, Atomic Energy of Canada Limited, Chalk River Nuclear Laboratories, Chalk River, Ontario, Canada

This review outlines progress in the development of SEM electron channelling pattern techniques since Coates first observed patterns and Booker *et al.* explained their origin ten years ago. Discussions are included on the mechanism of electron channelling in crystals, electron optical and specimen conditions for generating patterns, pattern indexing, selected-area analysis, and applications. Progress in revealing crystal defects is also discussed.

1. Introduction
Ten years ago, Coates [1] noted some unusual features on his scanning electron microscope (SEM) images; lines and bands of contrast, superimposed on topographical features of cleaved GaAs crystals. He termed these "Kikuchi-like" reflection patterns, because of their geometrical similarity to transmission and reflection Kikuchi patterns, and showed that they could be used to orient single crystals. Subsequently, Booker *et al.* [2] confirmed Coates' observations and explained them in terms of the electron channelling model previously advanced by Hirsch *et al.* [3] to predict the orientation dependence of X-ray emission from thin crystals [4]. Thus, the "electron channelling patterns" (ECPs) were simply another manifestation of an already well-understood phenomenon. Their occurrence, however, was of practical interest, because bulk specimens could now be crystallographically examined while viewing them directly, thereby allowing such possibilities as rapid orientation determination, dynamic recrystallization studies and assessment of crystal surfaces. Furthermore, as recognized both by Coates and Booker *et al.*, the possibility arose of examining selected areas as small as the beam diameter, which would permit studies on the microstructural scale. In addition, defect detection seemed feasible [2].

During the past decade, advances have been made both in the theoretical and in the practical aspects of SEM-ECPs. The purpose of this paper is to review these developments. The approach is pedagogical to some extent, in order to introduce the ECP technique to prospective users.

2. Principles of Scanning Electron microscopy
Before embarking on the main theme, it is appropriate to briefly outline the principles of scanning electron microscopy [5, 6]. As shown in Fig. 1, electrons from a cathode, C, pass through a series of lenses, L, and focus on the surface of a specimen, S. A portion of the electron current leaving S is collected by a detector, P, and then passed to an amplifier, A, the output of which modulates the brightness of a CRT display. As the beam passes along the column, it is deflected in two mutually perpendicular directions by a set of scanning coils, D, as shown in Fig. 2. The beam deflection is synchronized with the spot on the CRT display so that a one-to-one correspondence exists between the beam position on S and the position of the spot on the CRT. In this way, an image is produced. Generally, the two main parameters of concern are the probe diameter at the specimen surface, and the probe current. The first of these limits the spatial resolution and

© 1977 Chapman and Hall Ltd. Printed in Great Britain.

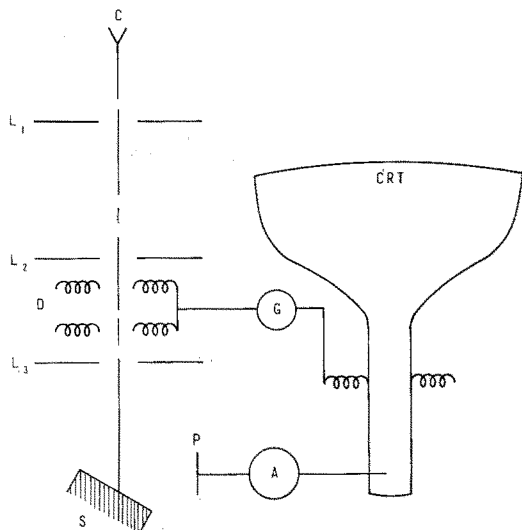

Figure 1 Schematic diagram of an SEM; C is the cathode, L the lens, D the deflection coils, S the specimen, P the detector, A the amplifier, G the scan generator.

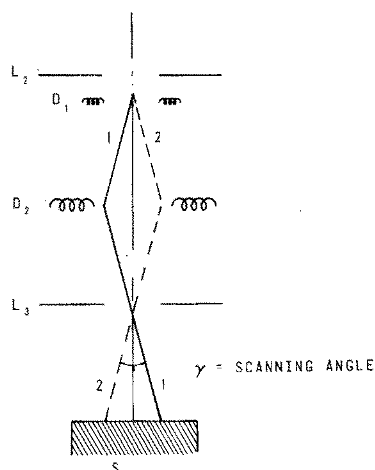

Figure 2 Schematic diagram of SEM double-deflection system. Note total scanning angle, γ. Positions 1 and 2 show that centre of the beam at time 1 and time 2, respectively.

the second, the contrast resolution. When dealing with channelling effects, a third point must also be considered, namely, the probe divergence. As will be discussed in Section 5, this limits the angular resolution of ECPs and, hence, the accuracy of the crystallographic information so obtained.

In addition to the further optical requirements, the use of the SEM in the ECP mode requires that the image be viewed in a different manner. Instead of regarding each point on the CRT display as corresponding only to a particular point on the specimen surface, each display point is related to a particular direction of incidence. The reasons for this are discussed in Section 4. Indeed, in the case of selected-area patterns (Section 10) each point in the display corresponds only to a particular direction of incidence, the point of incidence on the specimen being fixed by de-activating the lower set of scanning coils (Fig. 2) and using the final lens to deflect the beam back to a point on the optic axis [7]. Thus, the total scanning angle, γ (Fig. 2), is also important.

3. Mechanism of electron channelling in crystals

3.1. Qualitative model

Energetic electrons (~20 kV) incident at near to a Bragg angle excite one strongly diffracted beam in the crystal. As discussed by Hirsch *et al.* [8], the subsequent motion through the lattice can be described as the sum of two Bloch waves, Fig. 3. These are plane waves modulated by the periodic potential of the crystal lattice: Wave 1 is modulated laterally with nodes at the atomic positions, whilst wave 2 has anti-nodes over the atomic positions.

Each wave scatters as it passes through the lattice. The scattering coefficient for wave 1 will be less than that for wave 2 because the current maxima avoid the atomic scattering sites. For each wave, the amplitude and scattering coefficient vary with the direction of the incident beam. Both waves are excited with equal amplitude when the beam exactly satisfies the Bragg condition $\mathbf{S_g} = 0$, where $\mathbf{S_g}$ is the deviation vector in reciprocal space in terms of the reflecting sphere parameters ($\mathbf{S_g} = \mathbf{g}\,\Delta\theta_B$ where $\Delta\theta_B$ is the actual deviation from the Bragg angle and $\mathbf{g}$ is the reciprocal lattice vector of the reflecting plane). The current flow is parallel to the planes and thus the scattering coefficients for waves 1 and 2 are respectively minimized and maximized. When the angle of incidence is greater than the Bragg angle ($\mathbf{S_g} > 0$), wave 1 is excited preferentially and when it is

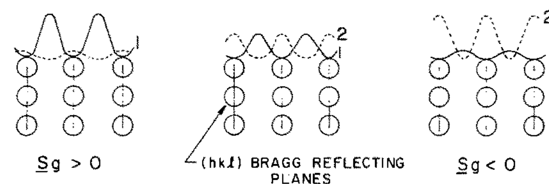

Figure 3 Sketch of Bloch waves 1 and 2. The circles represent atoms. $\mathbf{S_g}$ is the deviation vector indicating the angular deviation from the exact Bragg reflecting condition.

less than the Bragg angle ($\mathbf{S_g} < 0$) wave 2 is excited preferentially. In these cases the current flow is not parallel to the reflecting planes, and the scattering coefficients for waves 1 and 2 increase and decrease respectively. Fig. 4 shows these variations qualitatively.

Because the Bloch wave amplitudes and scattering coefficients vary about the Bragg position, electron scattering in crystals is a function of the direction of incidence. For $\mathbf{S_g} > 0$, scattering is reduced; the electrons channel into the lattice and thus have reduced probabilities of being back-scattered through the surface of incidence. For $\mathbf{S_g} < 0$, scattering is enhanced, because in this case the incident beam produces more back-scattering electrons from the region nearer to the surface which thus have a greater chance of escaping. It follows that as the incident beam passes through a Bragg position the total intensity $I_B(0)$, of the electrons back-scattered through the entry surface will be modulated: for $\mathbf{S_g} > 0$ the intensities will be less than background, while for $\mathbf{S_g} < 0$ they will be greater.

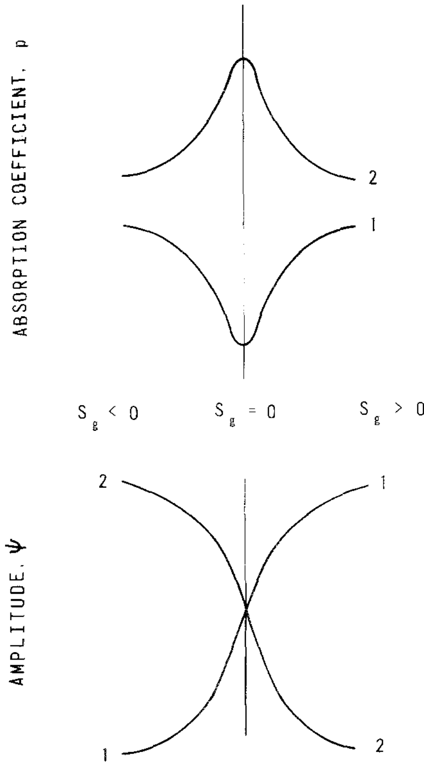

Figure 4 Sketch of Bloch wave absorption coefficients and wave amplitudes versus the deviation vector (2-beam approximation).

3.2. Quantitative model

Detailed theories by Hirsch and Humphreys [9], Vicario *et al.* [10], Spencer *et al.* [11] and Sandström *et al.* [12] have been developed to explain the quantitative variation in $I_B(0)$ with the direction of incidence. These express the incident electron wave function within the crystal, not in terms of only two Bloch waves, but by a linear superposition of Bloch waves, of intensity

$$I^{(j)}(x) = I^{(j)}(0) \exp(-\mu^{(j)}x)$$

where x is the distance beneath the entrance surface, $I^{(j)}(0)$ is the intensity of Bloch wave j at the surface ($x = 0$) and $\mu^{(j)}$ is the corresponding absorption coefficient. By dividing the electrons which have been removed from wave j into those back-scattered, $I_B^{(j)}$, and those forward-scattered, $I_F^{(j)}$, and by considering a slice of crystal of thickness dx at a depth x beneath the surface, irradiated by three categories of electrons of intensity $I^{(j)}(x)$, $I_B^{(j)}(x)$ and $I_F^{(j)}(x)$ respectively, differential equations can be derived for $dI_B^{(j)}$ and $dI_F^{(j)}$ which contain the back-scattering coefficients ($p^{(j)}$ for Bloch wave (j) and $p^{(0)}$ for the plane waves corresponding to $I_B^{(j)}$ and $I_F^{(j)}$). Solution of these equations gives $I_B^{(j)}(0)$, the back-scattered intensity at the entrance surface due to electrons originally associated with Bloch wave (j). Hence

$$I_B(0) = \sum_j I_B^{(j)}(0).$$

While multi-beam calculations of this type are necessary for complete determination of $I_B(0)$, the general behaviour around a Bragg position can be understood from the two-beam argument discussed by Schulson [13]. In this approximation

$$I_B(0) \propto 1 - \frac{\chi_g}{1 + \chi_g^2} \tag{1}$$

in which $\chi_g = \mathbf{S_g}\ \xi_g$, where ξ_g is the extinction distance for the reflection excited. Equation 1 is plotted in Fig. 5, which is the backscattered analogue of the transmission electron microscopy "rocking curve": for $\chi_g > 0$, $I_B(0)$ is less than the background value, and for $\chi_g < 0$, $I_B(0)$ is greater, as observed experimentally. This description also leads to an expression for the angular width, $2\omega_g$, of the corresponding channelling line defined as the spread in directions of incidence $\delta(\Delta\theta)_g$ corresponding to the range $\delta\chi_g = 2$ within which $I_B(0)$ goes from a minimum to a maximum. Thus

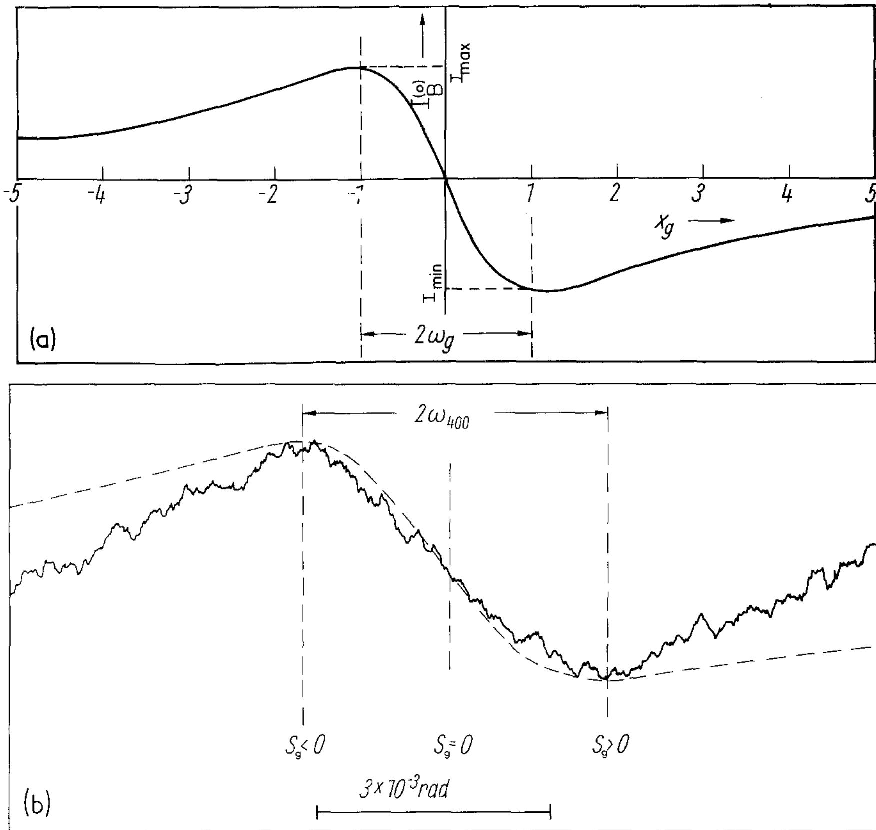

Figure 5 Back-scattered electron intensity about an SEM electron channelling line (relative variation). (a) Calculated; $2\omega_g$ – line width (b) Measured profile for 25 kV – (400) reflection in silicon [13]. (Reproduced with permission from Akademic-Verlag, Berlin.)

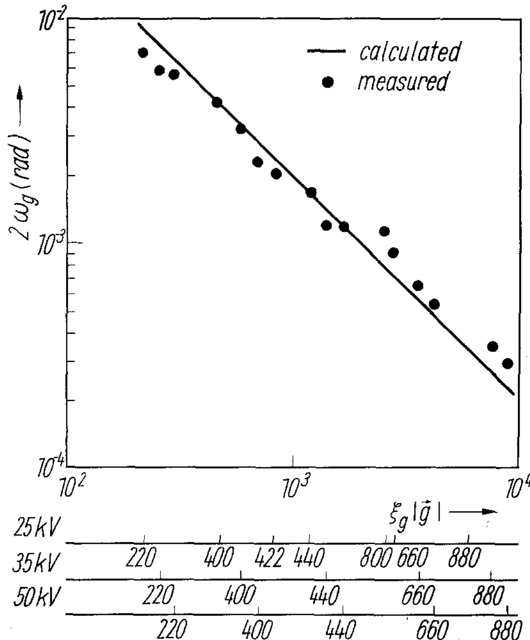

Figure 6 Experimental and calculated widths for SEM electron channelling lines [13]. (reproduced with permission from Akademi-Verlag, Berlin.)

$$2\omega_g = \frac{2}{\xi_g|\mathbf{g}|} \tag{2}$$

From the two-beam approximation then, it can be seen that the channelling lines rapidly become narrower with increasing **g**, which is in quantiative agreement with measurements for silicon using 20 kV electrons as shown in Fig. 6. For heavier elements and more energetic electrons, multi-beam effects become important, and so departures from the two-beam approximation are to be expected.

4. General aspects of SEM–ECPs

4.1. The SEM geometry and ECPs

We shall now show how ECPs are generated in the SEM. Fig. 7 illustrates the principle for a single crystal, having one set of Bragg planes perpendicular to its surface upon which a well-collimated, monochromatic beam of energetic (say 20 kV) electrons is incident. Although a scanning beam is shown, the principle is the same for a rocking beam.

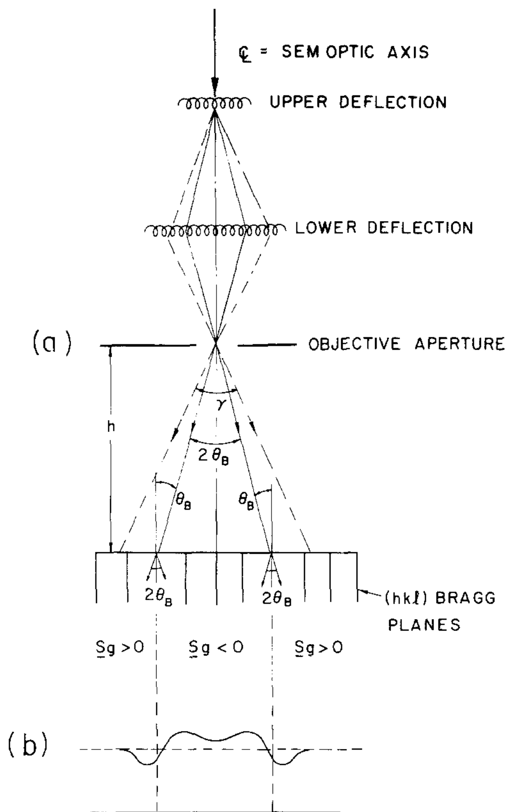

Figure 7 Schematic diagram of SEM geometry for generating electron channelling patterns.

In terms of the two-beam approximation, two Bloch waves are excited in the crystal as the incident beam approaches the exact Bragg reflecting position. As described in Section 3, the back-scattered signal is modulated, and that part of the secondary electron signal which is created by back-scattered electrons is similarly affected. Because the scan is symmetrical relative to the planes shown, the beam passes through the Bragg position twice (each time it sweeps the surface in the direction indicated). Two symmetrical electron channelling lines are thus produced. One corresponds to scattering by the "front-side" of the Bragg planes, (hkl), and the other to scattering by the "back-side", $(\bar{h}\bar{k}\bar{l})$. If the spacing between the planes (in real space) is sufficiently large, then the Bragg angle will be small enough to allow the signal from the two channelling lines to overlap. This produces a channelling band, brighter than background, bordered by edges darker than background. In terms of the previous notation, the bright regions correspond to directions of incidence for which $\mathbf{S_g} < 0$ and the dark, to directions for which $\mathbf{S_g} > 0$.

Fig. 8 illustrates these points. Because the incident beam generally scans through more than one set of Bragg reflections during a complete frame scan, more than one pair of parallel lines (or bands) is usually generated. The totality of such lines and bands is referred to as an electron channelling pattern. The one shown is a ⟨1 1 1⟩ pattern from silicon, generated using 20 kV electrons; the three main bands result from {2 2 0} reflections. For such images, the larger the scan

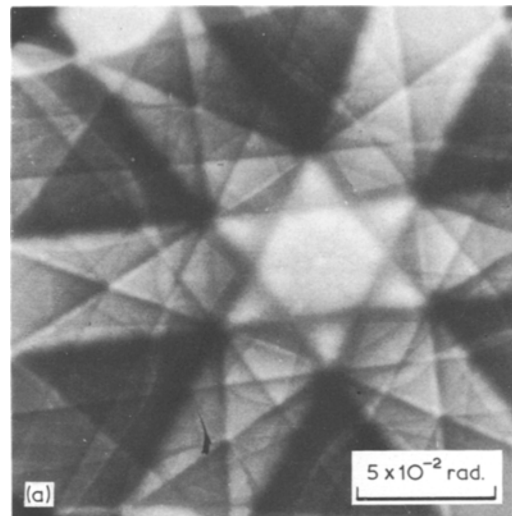

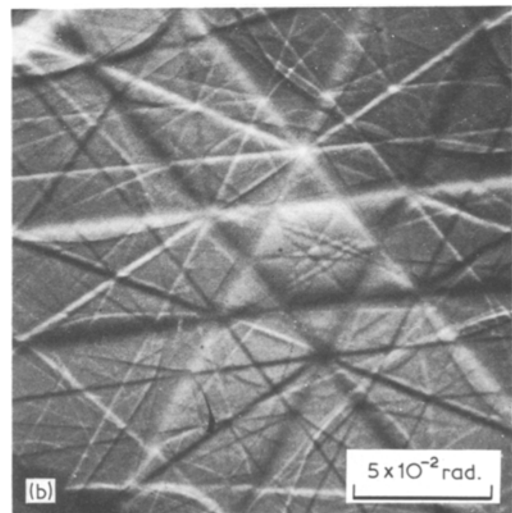

Figure 8 SEM-electron channelling patterns from a (1 1 1)-oriented silicon single crystal, generated using a collimated beam and collecting the back-scattered signal (20 kV electrons): (a) Collected electron image, (b) differentiated collected electron signal with respect to time. (These patterns were generated using the Stereoscan SEM at Oxford University by C.G. van Essen and the author, 1969).

angle (i.e. the lower the magnification setting), the greater is the number of lines in the pattern.

4.2. Characteristics of the patterns

It follows that ECPs behave as though they are attached to the crystal lattice; that is, upon displacing the crystal, the pattern remains unchanged, but upon rotating or tilting the crystal, the patterns rotate or tilt accordingly, the latter operation resulting in a new pattern. It also follows that the width of a channelling band is directly proportional to both the Bragg angle and the wavelength λ of the incident electrons. These features allow pattern geometry to be used to determine crystallographic orientations and lattice parameters, a subject discussed more fully in Section 7.

It is evident from the Bloch wave model that distortions of the lattice planes lead to local variations in the degree of electron channelling and scattering. Consequently, crystalline defects having an associated strain field (such as dislocations), or mosaic spread in single crystals, lead to pattern blurring. As the ECP quality is measured in terms of the angular width of a channelling line, usually the narrowest one on the pattern, (or in terms of the signal from a given channelling line, $I_{max}-I_{min}$, as in Fig. 5a) the pattern is thus sensitive to crystalline imperfections. This point is discussed again in Section 8.

4.3. Information depth

As the electrons propagate through the lattice, they are scattered out of the Bloch wave states, resulting in fewer electrons retaining their original identity. Eventually all the electrons lose their Bloch wave character and, on average, behave as plane waves [9]. Their energy, however, is still sufficient to allow propagation to even greater depths. Consequently, back-scattering continues even though channelling stops. It thus follows that that part of the back-scattered signal which is orientation-dependent comes from those electrons which travel only a short distance into the crystal before being back-scattered: those penetrating to greater depths contribute only to the background signal.

Calculations [9] indicate that for bulk specimens of silicon, for instance, the channelling signal $I_{max}-I_{min}$ generated using 20 kV electrons (Fig. 5) originates within the first 100 nm of material, the major part coming from the upper 50 nm. For heavier elements and for lower energies, the "information depth" is even less.

4.4. Collected signals and signal processing

Patterns can be generated either by collecting the back-scattered and/or secondary electron signals, or by collecting the specimen current. In the latter case, contrast is reversed: the bands are darker than background, and the edges lighter. In cathodoluminescent materials such as CdS, patterns can also be observed by monitoring the emitted light [14].

In an earlier review [6], Booker discussed signal processing which makes use of the fact that the SEM signal varies with time. Two useful procedures for visibility enhancement are (i) backing off the d.c. level of the signal and increasing the amplifier gain, and (ii) pattern sharpening by differentiating the signal with respect to time. Two points to note regarding time differentiation are that it results in channelling lines parallel to the CRT line scan being lost, and channelling bands perpendicular to the line scan, which originally have symmetrical contrast, show asymmetrical contrast [15].

5. Electron optical conditions for ECP generation

Three parameters are important, the probe current at the specimen surface i, the probe divergence δ, and the probe diameter l. These are related through the brightness B of the electron optical system, which is constant along the optic axis [6], and is given by

$$B = \frac{0.4i}{l^2 \delta^2}. \tag{3}$$

For conventional tungesten hairpin filaments of the type commonly used in commercial SEMs, $B \simeq 2 \times 10^4$ A cm^{-2} sr^{-1} at 20 kV. The probe current is important because it determines the level of contrast that can be detected for a given scan time. Remember that from the theory of image formation [5], the higher the signal to noise ratio S/N, the lower the level of contrast that can be detected. To a first approximation, $S/N \propto i^{1/2}$. Divergence is important because, in the absence of crystal distortions, it determines the sharpness of a channelling line: clearly, the more nearly parallel the beam, the greater the number of

electrons which fall within the range ($\mathbf{S_g}$, $\mathbf{S_g} + \delta \mathbf{S_g}$), where $\delta \mathbf{S_g}$ corresponds to a range of angles of incidence $\delta\theta$). Finally, l is important in the "selected area" mode of operation (Section 10), because it sets the theoretical limit on the size of the selected area.

5.1. Probe current

Considerations of signal/noise ratio [16] show that the probe current i_c required to detect a given level of contrast C, is proportional to C^{-2} If C in the present instance is defined from Fig. 5 as $C = (I_{max} - I_{min})/0.5(I_{max} + I_{min})$ it follows that

$$i_c \propto 1/(I_{max} - I_{min})^2;$$

the lower the channelling signal, the higher the beam current needed to detect it. Generally, $(I_{max} - I_{min})/0.5(I_{max} + I_{min})$ is observed to be less than $\simeq 0.1$, which means that the beam current must be greater than $\simeq 10^{-9}$ A to see channelling contrast. Under conditions of high-resolution topographical imaging, $i \simeq 10^{-11}$ to 10^{-12} A in which case channelling contrast cannot be seen. Fig. 9 illustrates these points.

Recent energy-loss calculations by Sandstrom *et al.* [12] show that optimum channelling contrast should be obtained by collecting back-scattered electrons of energies E within the window $E_0 > E > E_0 - \Delta E_w$, where E_0 is the incident beam energy and ΔE_w is the window width, and where for 20 kV electrons ΔE_w(eV) = 700 for Si, 250 for Cu, and 400 for Au. Effectively, this means that beam currents of an order of magnitude lower would be required to display the same contrast which can now be observed using non-discriminating detectors. It also means that individual crystal defects should be more easily detected (Section 9).

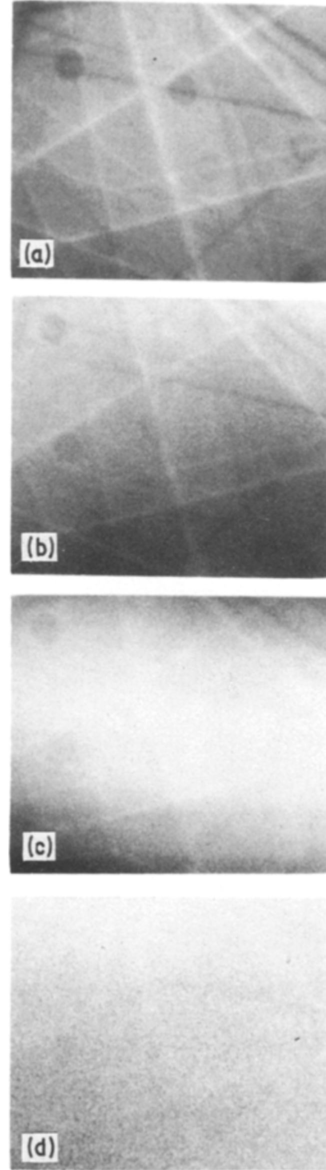

Figure 9 ECPs from a silicon single crystal showing the effect of beam current on pattern detection. The patterns were obtained using the JSM-11-SEM. The beam current was changed by varying the filament current and measured using a specimen current amplifier (25 kV electrons; $\delta \simeq 3 \times 10^{-4}$ rad). Note the loss of electron channelling contrast for $i < 2 \times 10^{-9}$ A. Beam current (A): (a) 2×10^{-8}, (b) 6×10^{-9}, (c) 2×10^{-9}, (d) 6×10^{-10}.

5.2. Probe divergence

From the discussion on line width, it follows that to detect a given channelling line $\delta \lesssim 2\omega_g$. In practice, this means that $\delta \lesssim 10^{-3}$ rad. Greater divergence leads to line blurring, as seen in Fig. 10. Procedures for varying δ are described in Section 5.4. and generally involve either changes in condenser lens settings or changes in the final aperture size.

5.3. Probe size

Equation 3 can now be used to estimate the diameter l_{min} (at the specimen surface) within which enough well-collimated electrons from the beam fall to allow ECPs to be generated in reasonable times. For conventional SEMs ($B \sim 10^4$ A cm^{-2} sr^{-1} at 20 kV)

$$l_{min} > \left(\frac{0.4 \times 10^{-9}}{(10^{-3})^2 \times 2 \times 10^4}\right)^{1/2} > 1.4 \times 10^{-4} \text{ cm.}$$

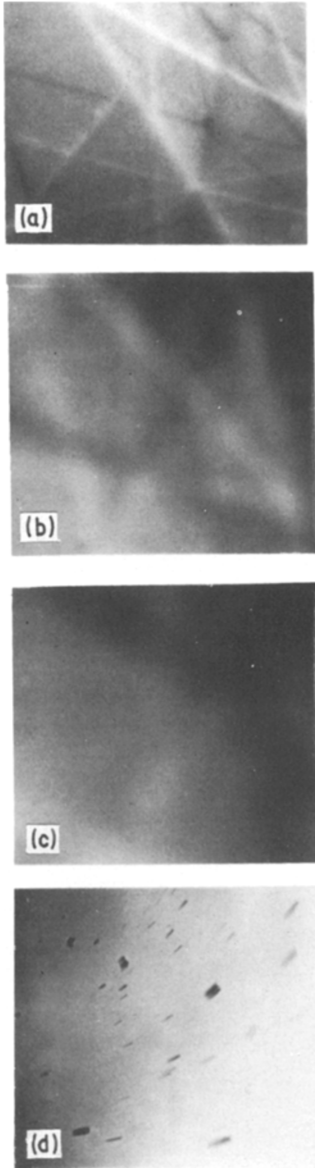

Figure 10 ECPs from a silicon single crystal showing the effect of beam divergence on angular resolution. The divergence was varied by altering the size of the final aperture while the beam current was held constant by varying the setting of the upper condenser lens (25 kV electron; $i \sim 10^{-7}$ A) Note the "bleaching out" of the pattern for $\delta > 10^{-3}$ rad. Beam divergence (rad): (a) 5×10^{-4}, (b) 5×10^{-3}, (c) 1×10^{-2}, (d) 1×10^{-1}

This result implies that

(i) only coarse topographical features can be simultaneously resolved when generating ECPs by scanning the probe across the crystal surface: the higher the angular resolution of the pattern (i.e. the smaller δ, for a given probe current), the large the probe diameter and hence the lower the spatial resolution;

(ii) to obtain both high angular and spatial resolutions higher brightness electron sources are needed. For example, a field emission source of $B \sim 10^7$ to 10^8 A cm^{-2} sr^{-1} should in principle allow an angular resolution of 10^{-3} rad and a spatial resolution of 10 to 50 nm;

(iii) the minimum area from which rocking-beam, selected-area patterns can be generated is of the order of 2 μm^2 (Section 10).

5.4. Procedures for setting up ECP optics

The optical condition necessary for ECPs can usually be established with suitable condenser lens settings and final aperture sizes. Three separate beam geometries can be set up; focused beam, unfocused beam, and collimated beam. Fig. 11 illustrates these and defines the beam divergence for each case. Each geometry requires different lens settings. Schulson and van Essen [17] described the underlying principles and listed lens settings for each case in the "Cambridge Instruments" – Stereoscan SEM, and Schulson applied the same analysis in the "JEOL" – JSM-II SEM [18]. The wide, collimated beam gives the highest ECP angular resolution and integrates out spatial information from the image. For any SEM, the simplest geometry is the unfocused beam, established by turning off all the lenses and using the normal ($\simeq$ 100 μm diameter) final aperture.

When generating ECPs for the first time, it is important to first analyse the optics of the instrument. The appropriate lens settings for the particular beam geometry required can usually be derived using the basic lens law

$$\frac{1}{u} + \frac{1}{v} = \frac{1}{f},$$

where u is the object distance, v is the image distance, and f is the focal length, and applying the expression for lens magnification $M = v/u$, and taking the size of the hairpin filament as $\simeq 50\,\mu$m. Clearly, the application of such an analysis depends upon the availability of data on focal length versus lens settings and the information on column geometry.

6. Specimen preparation for generating ECPs

In Section 4 we noted that only electron scattering within the top hundred or so atomic planes gives

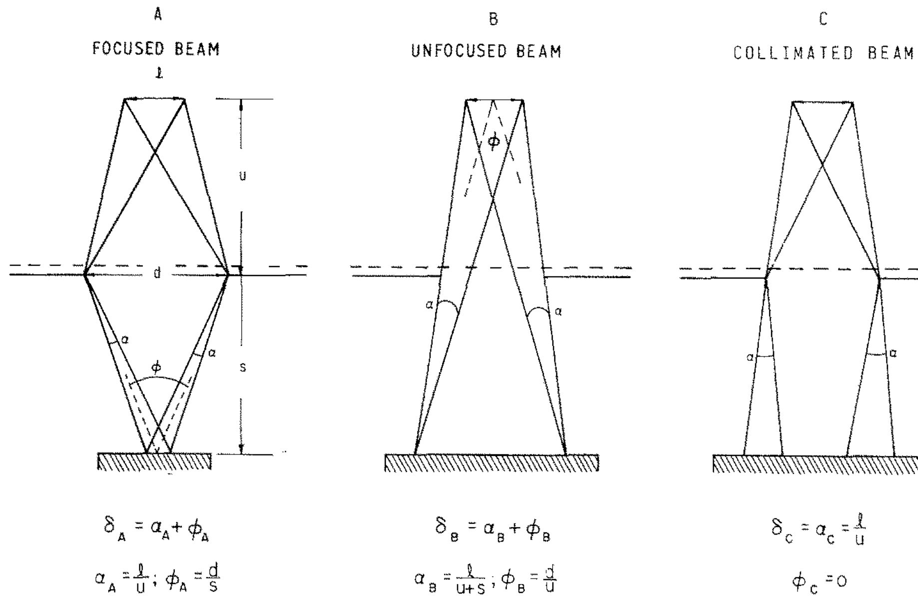

Figure 11 Sketch of three different types of electron channelling beams with definition of beam divergence, δ.

rise to the electron channelling contrast, even though a 20 kV electron penetrates to depths of 1 to 2 μm. Surface condition, therefore, is important.

Surfaces must be free from excessive films (e.g. oxides) and from plastic deformation (such as that due to mechanical polishing). Films cause a general blurring or loss of contrast, while plastic deformation causes line broadening and attendant reductions in contrast [14, 19]. A simple guide is that the thickness of heavy films (e.g. oxides of metals of high atomic number) should be $\leqslant 5$ to 10 nm, and of light films $\leqslant 10$ to 20 nm. Fig. 12 illustrates these points for carbon on silicon and anodic tungsten oxide on tungsten. It is also advisable that the test surfaces should be chemically rather than mechanically prepared. This precaution is particularly important when examining "soft" metals (e.g. Al, Cu, Au), because in these cases the author has found that even abrasives as fine as 0.05 μm alumina can cause sufficient surface deformation to completely obliterate ECPs. It is also advisable to chemically prepare surfaces shortly before the examination, since oxides formed during one or two day exposures to laboratory environments can lead to considerable loss of contrast.

In addition to surface condition, internal distortions also lead to reductions in pattern contrast. For example, a compressional strain of $\simeq 0.2$ greatly reduces the "recognizability" of ECPs from a Cu–10 wt % Al alloy, while a strain of $\simeq 0.4$ leads to complete loss of crystallographic identity [14]. Similar effects occur in 316 stainless steel [19]. Thus, it is not useful to examine highly deformed materials.

The author has found that, when examining insulating crystals, a useful procedure is to use a very rapid framescan. Otherwise, large surface electric fields develop which lead to pattern distortion. In the case of materials such as alkali halides which are susceptible to ionization damage, examinations could be made using a heating stage, by operating at temperatures above the annealing temperature for radiation damage.

7. Indexing ECPs

Pattern geometry may be viewed as a crystallographic "finger-print". Correct indexing allows orientation and lattice parameter determinations and, in principle, crystal identification. Both analytical and comparative procedures for these purposes have been developed [20, 21].

7.1. Analytical methods

If the width of an (hkl) electron channelling band is W (see Fig. 13), the length of the display tube raster D, and the scanning angle (in one-dimension) γ, then the corresponding Bragg angle is

$$2\theta_B = \frac{W}{D}\gamma. \quad (4)$$

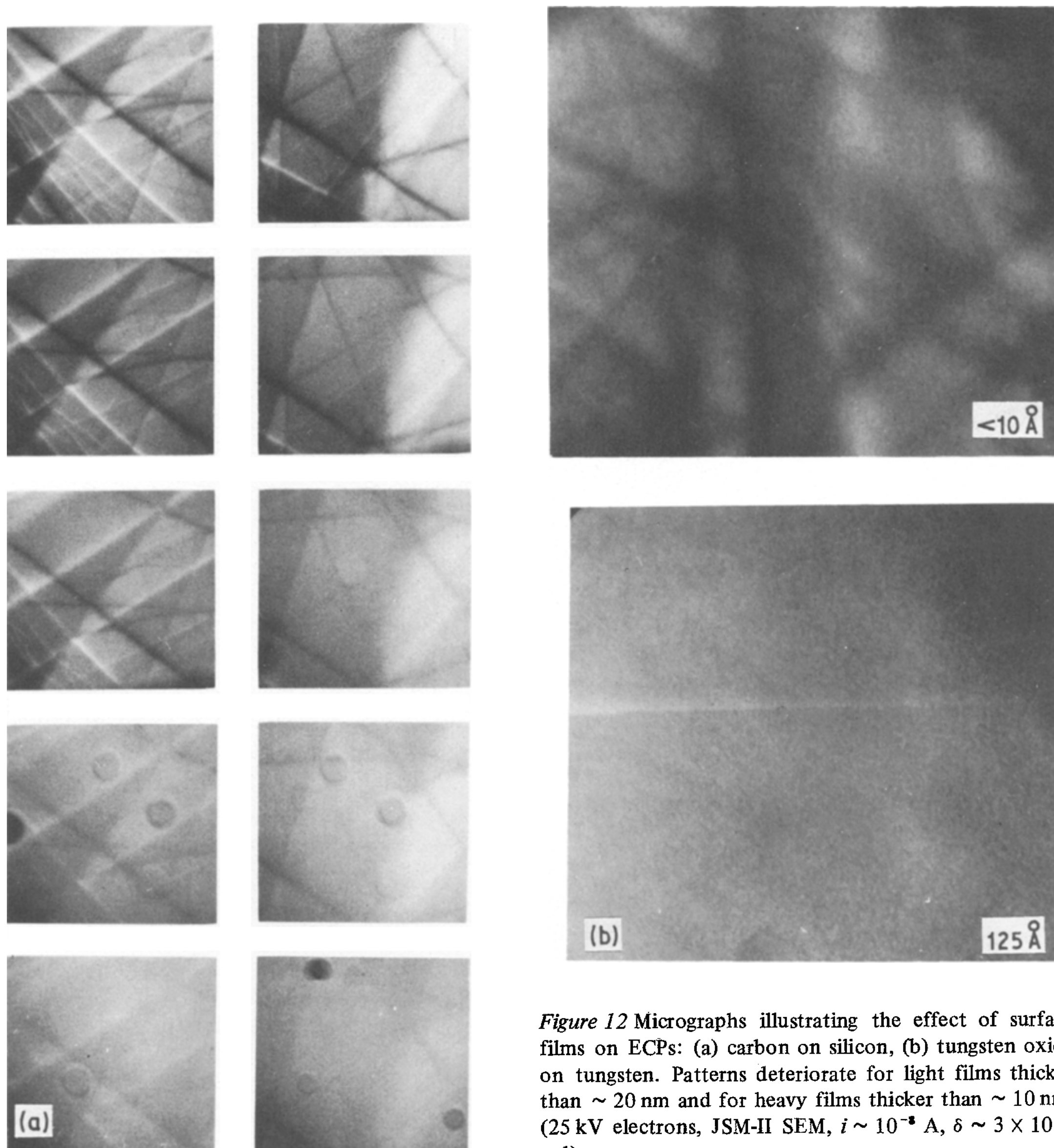

Figure 12 Micrographs illustrating the effect of surface films on ECPs: (a) carbon on silicon, (b) tungsten oxide on tungsten. Patterns deteriorate for light films thicker than ~ 20 nm and for heavy films thicker than ~ 10 nm. (25 kV electrons, JSM-II SEM, $i \sim 10^{-8}$ A, $\delta \sim 3 \times 10^{-4}$ rad).

From Equation 4 and Bragg's law it follows that

$$d_{(hkl)} = \frac{D\lambda}{W\gamma} \tag{5}$$

where $d_{(hkl)}$ is the interplanar d-spacing for the (hkl) reflecting planes. Thus, a complete set of d-spacings can be generated and the crystal form identified using standard procedures.

Prior to further discussion two practical points should be noted:

(i) Although the lines which form an ECP appear to be straight, they are, in fact, slightly curved and represent the intersections of cones with imaginary planes. Thus, measurements of the width W between channelling line pairs should be made along a direction normal to each line and passing through the centre of the image. Preferably, measurements should be made between pairs of higher index reflections situated on either side of the main band since these are sharper.

(ii) The scanning angle γ is obtained experimentally [22] by measuring the displacement ΔS of an electron channelling pattern corresponding to the change in the amount of specimen tilt, $\Delta\beta$, about an axis normal to the undeflected incident beam. This is equivalent to measuring the

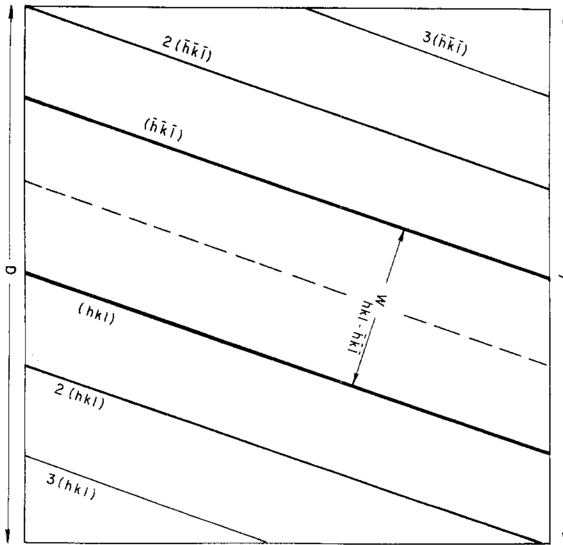

Figure 13 Diagram of SEM electron channelling pattern illustrating relevant parameters for band indexing by analytical methods.

displacement of points of intersection for two or more channelling lines. Thus

$$\gamma = \frac{D}{\Delta S}\Delta\beta. \tag{6}$$

Schulson [22] has discussed both of these points in more detail.

Having assigned (hkl) indices to channelling bands by width measurements, a useful check is to measure the inter-band angles (preferably by locating the pole at the centre of the image). These correspond to the interplanar angles of the related reflecting planes. A glance at a table of interplanar angles will then either confirm or refute the previous indexing scheme.

Often, only un-paired channelling lines are seen on an ECP. In such cases the lines may be indexed using a differential method of analysis [20]. Rewriting Equation 5 for W and differentiating with respect to λ gives

$$\frac{\mathrm{d}W}{\mathrm{d}\lambda} = \frac{D}{d_{hkl}\gamma}. \tag{7}$$

Thus a change in the beam energy corresponding to a change $\Delta\lambda$, also causes a change in the width of a channelling band, ΔW. In other words, each line making up the band moves a distance $\Delta W/2 = \Delta Y$. Thus, by measuring the movement (along a direction normal to the line) following a change in beam energy, the d-spacing of the corresponding reflection can be calculated using the expression

$$d_{(hkl)} = \frac{D}{\gamma}\frac{\Delta\lambda}{2\Delta Y}. \tag{8}$$

A practical point to note from Equation [8] is that the more closely spaced the reflecting planes (i.e. the smaller d and, hence, the higher the corresponding (hkl) indices), the larger the shift of the (hkl) channelling line. This point is of qualitative assitance when indexing patterns.

Based on the differential method, a computer program has been developed for pattern indexing [23].

In the description of the differential technique we have assumed that the scanning angle does not change on changing the beam energy. In some SEMs this is the case. In other, however, it is not and in such instances corrections must be applied before using the method.

7.2. Comparative methods

ECPs can be indexed by using Kikuchi maps obtained from electron diffraction experiments on thin crystals having the same structure. However, while the overall geometry of ECPs and Kikuchi maps is similar, the detailed structures differ. For instance Kikuchi maps are usually generated using 50 to 100 kV electrons, whereas channelling maps are obtained using 10 to 30 kV electrons. As a result, the angular width of an (hkl) channelling band is larger than that of the corresponding Kikuchi band and consequently detailed comparisons between the two types of map are not justified.

A better way is to compare the pattern to be indexed with an ECP map. This is a stereographic representation of ECPs for all orientations generated. Fig. 14 shows an ECP map for 20 kV copper reflections [24]. ECP maps have also been published for niobium–15 kV [21], silicon–20 kV [20] and molybdenum–20 kV [25].

8. Quality of ECPs

As noted in Sections 4 and 6, ECPs are sensitive to lattice imperfections. Thus, in principle, it should be possible to extract structural information such as dislocation content. This is a point of particular interest and is discussed again in Section 9. In practice, however, progress in this direction has been difficult, and as yet angular resolution and line contrast are regarded as only of qualitative value. Nevertheless, this aspect of ECPs is useful in evaluating relative changes in lattice

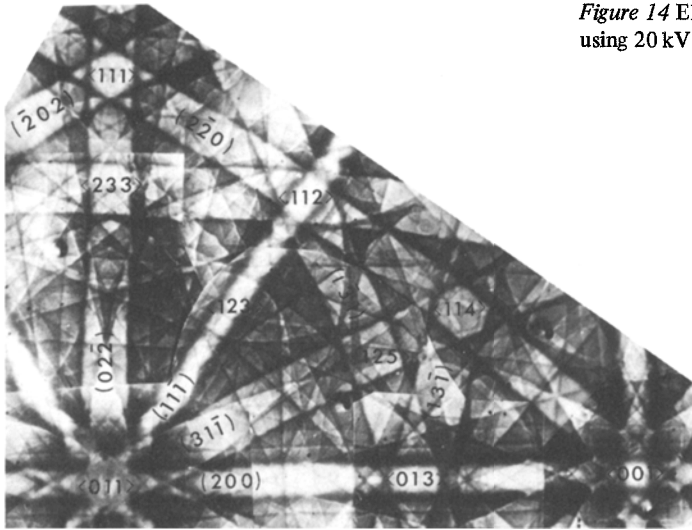

Figure 14 Electron channelling map for copper generated using 20 kV electrons [24].

perfection which arise, for example, through ion implantation [26–28] or plastic deformation [19]. Qualitative aspects may also be useful when following the early stages of film growth.

For practical purposes, pattern contrast is taken as the contrast of the lowest index (i.e. broadest) line on an ECP, for example, the (220) line for silicon; pattern resolution is the angular width of the narrowest line detected. Contrast can be measured by scanning across the channelling line in question and displaying the detector output on an oscilloscope. Alternatively [16], it can be calculated from the relationship $i_c \propto C^{-2}$ (Section 5.1), where i_c is obtained by turning down the incident beam current until the line of interest can just be detected above background. Resolution is measured from micro-densitometer traces across ECP negatives.

More important from a practical point of view are changes in pattern quality. These can be correlated with known values of film thickness (oxidation and epitaxial growth studies), plastic strain (deformation studies) or irradiation damage (ion implantation of semiconductors), and then used to measure these parameters in test specimens. Changes in quality are easily measured using the critical beam current method [16]. The procedure is to measure the critical beam current for a given (hkl) line as a function of film thickness, strain, etc. From the critical current for the same line in a reference specimen, it is then possible to obtain the reduction in contrast R given by

$$R = 1 - (i_c^r/i_c^t)^{1/2}, \qquad (9)$$

where i_c^r and i_c^t are the critical currents for the reference and test states, respectively. ([28] contains a worked example of this procedure.)

9. Crystal defects

Because microstructure and material properties are often intimately related, it is essential to one's understanding of material behaviour to have a clear description of microstructural features. Classically, optical microscopy has provided such information and, more recently, transmission electron microscopy. It now seems possible that scanning electron microscopy of bulk samples might also assist in this regard. Already, it is a simple matter to reveal the presence of grain boundaries in unetched polycrystals by using the focused channelling beam geometry (Fig. 11c). In this case, the contrast arises from the different orientations of each grain on either side of a boundary; work is in progress to investigate crystal defects. Indeed, Clarke [29], Stern *et al.* [30], and Booker *et al.* [31] have revealed dislocation and stacking faults in thin foils using the back-scattered, SEM mode of using a conventional TEM – important first steps in resolving such features in bulk materials.

As discussed by Booker [6], and quantified by Clarke and Howie [32], and Humphreys *et al.* [33], dislocations emerging at the surface cause the lattice planes to be bent locally and hence give rise to local changes of orientation. Second phase particles, near-surface radiation damage, and recrystallization nuclei should cause similar changes. To see such bending, the specimen should be set near a Bragg reflecting posi-

tion, the idea being that the strain field from the defect should effectively produce a change in the deviation vector, δS_g and thus lead to electron channelling contrast when examining the surface using a well-focused probe. The first attempts to test these ideas, however, were unsuccessful.

The difficulty is easy to appreciate from the discussion in Section 5. To detect channelling contrast, it is now known that a probe of at least 10^{-9} A collimated at least to 10^{-3} radians is necessary. Moreover, to simultaneously resolve structural features on a scale of 50 nm (corresponding to the extent of the strain field about a screw dislocation within which the strain is > 0.001) the probe diameter must be 50 nm or smaller. Consequently, the beam brightness (Equation 3) must exceed 10^7 A cm^{-2} sr^{-1}. The brightness of most commercial SEMs, however, is only of the order of 10^4 to 10^5 A cm^{-2}, which accounts for the difficulty. Calculations [12] suggest that by using energy selecting detectors, a facility not available in most SEMs, the beam brightness required should be reduced by about an order of magnitude. Even so, filaments of higher brightness will still be needed if individual defects are to be observed in thick crystals. The problem is less serious in thin foils because the channelling contrast $C = (I_{max} - I_{min})/0.5(I_{max} + I_{min})$ (Fig. 5) is greater, due to the lower background 0.5 $(I_{max} + I_{min})$, while from the signal/noise argument in Section 5, when C is greater by a factor f, this is equivalent to the beam being brighter by a factor f^2.

The problem of resolving individual defects in bulk specimens thus remains an intriguing challenge. While the theories [32, 33] are now well advanced and lead to detailed predictions of the electron optical conditions for defect resolution, instruments with which to perform the experiments are not yet available. However, with the increased interest in cold-field electron sources of the Crewe [34] type (e.g. [35, 36]) one can look forward to the time when SEMs of the required brightness are coupled to energy selecting detectors, precision tilt stages and signal processing equipment in order to allow routine examinations of the type envisaged.

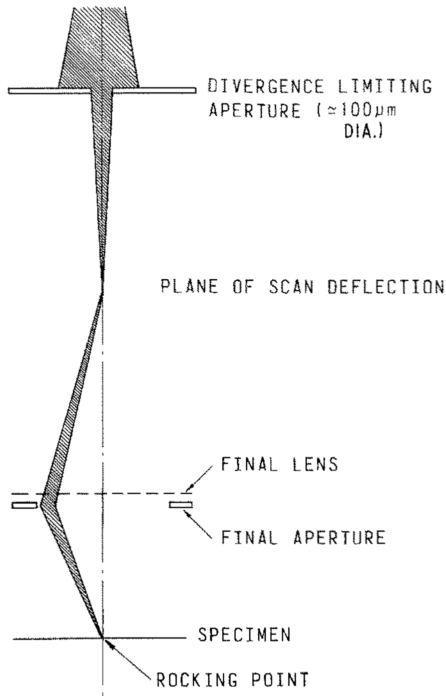

Figure 15 Diagram of the deflection-focusing method for rocking an electron beam about a fixed point on a surface. The final aperture is enlarged to $\simeq 1$ mm diameter to accommodate the probe travel in the plane of the final lens. The final lens acts to deflect the beam back to a point on the SEM optical axis and to simultaneously focus it.

10. Selected-area channelling patterns (SACPs)

A simple geometrical argument based on a working distance* of 10 mm and a scanning angle γ of $6°$ shows that the minimum area from which ECPs can be generated using a scanning beam is of the order of 1 mm^2. This section discusses a method for reducing the channelling region to a few μm in diameter in conventional SEMs.

10.1. The deflection-focusing method

As noted in Section 2, an essential feature for generating ECPs is a variation in the direction of the incident beam. In selected area work, this is effected by pivoting the probe about a fixed point on the specimen surface. The procedure developed by van Essen *et al.* [7, 24] is to deflect the beam once above the final lens and then to deflect it back to a point on the SEM optical axis while simultaneously focusing it using the final lens (Fig. 15). The point at which the beam crosses the axis is the rocking point, which is made coincident with the specimen surface. The diameter

*Working distance is defined as the distance between the cross-over point in the plane of the final lens and the specimen surface.

of the final aperture must be enlarged to $\simeq 1$ mm to accommodate the probe travel in the lens plane. Also, the aperture of the lens above the deflecting coils must be reduced to $\simeq 100\,\mu$m to reduce the probe divergence to $\simeq 10^{-3}$ rad.

To operate, the sample is first examined using a standard scanning beam and then the area of interest is translated to a predetermined spot on the viewing screen. On switching to the rocking beam mode an ECP appears.

All the considerations concerning electron optics and specimen preparations already discussed apply and, in addition, probe size must be considered.

10.2. Limitations on size of area analysed

Although the theoretical minimum area from which patterns can be generated is determined by beam diameter ($\simeq 1.4\,\mu$m, Section 5.3) the practical minimum area is limited by scan distortions. A "spherical aberration" occurs because the deflected beam does not intersect the optical axis at the same position for each direction of incidence; this aberration originates in the final lens. An "astigmatic" aberration may occur if the cross-over point for paraxial rays deflected in the X-plane is different from that for Y-deflections; this aberration originates in the scan coils if the X and Y deflecting pairs are not in the same plane. Consequently, the rocking-point is really a "disc of confusion" and larger than the theoretical minimum area.

Of the two, spherical aberration is usually the more serious. To a first approximation, therefore, the minimum practical diameter for selected area work may be expressed as

$$d_{\min} = (l_{\min}^2 + d_s^2)^{1/2}, \qquad (10)$$

where $l_{\min}$ is given in Section 5.3 and d_s is the diameter of the disc of confusion for spherical aberration, given by

$$d_s = \frac{1}{2} C_s \left(\frac{\gamma}{2}\right)^2, \qquad (11)$$

where C_s is the spherical aberration coefficient for the deflection-focusing lens. The value of C_s depends on the working distance and can be minimized by operating the lens at the shortest practical focal length. When this is done, $C_s \simeq$ 20 mm, implying that $d_s \simeq 1\,\mu$m for a scan angle of 6°, and thus $d_{\min} \simeq 2\,\mu$m. Experience has shown that the actual minimum diameter of pattern generation is about $5\,\mu$m, in fair agreement with the above analysis.

Equation 11 implies that d_s could be made insignificant with respect to a value of $l_{\min}$ of $1.4\,\mu$m by using $\gamma \simeq 3°$. This procedure has the disadvantage of reducing the number of lines and bands on the ECP, thus making pattern indexing more difficult. A better was to reduce d_s is described by van Essen [37]. He changed the form of the scan from saw-tooth to spiral; i.e. to a circular raster with a slowly changing diameter. In this way he and others [38] have generated ECPs from regions between 1 and $2\,\mu$m diameter, i.e. close to the theoretical limit.

It should be recognized that the limit of $\simeq 1\,\mu$m applies only when the beam brightness is around 2×10^4 A cm^2 sr^{-1}. If B were increased by a factor of 10^4, the theoretical limit would be reduced to about 10 nm.

10.3. Dependence of area size on rocking angle and working distance

When performing or designing SEM-SACP experiments it is useful to know values of d_s in advance. To obtain these, Booker and Stickler [39, 40] performed a detailed analysis of "spherical aberration" errors, giving particular values for stereoscan SEMs. Depending on the final lens setting and the rocking angle, d_s falls between 1 and $100\,\mu$m.

10.4. Some practical guides

(i) When operating at a small working distance (1 to 2 mm) use the specimen current to form the image. The geometry restricts efficient backscattered and secondary electron detection.

(ii) Use a fine-mesh (> 600 lines cm^{-1}) grid when first assessing the minimum useful area with an existing SEM. As the specimen and rocking "point" are brought into coincidence (either by altering the final lens current or by raising or lowering the specimen), the magnification will increase greatly causing either pincushion or barrel distortion. On passing through the rocking-point, the form of distortion will reverse.

(iii) Use a "good" single crystal when establishing the correct channelling beam conditions (i.e. $\delta < 10^{-3}$ rad and $i > 10^{-9}$ A). Polished silicon wafers are readily available and make excellent standards.

(iv) In practice, a useful indication of the actual rocking area is the size of the residual contamination mark.

11. Applications of SEM-ECPs

Table I summarizes successful SEM-ECP applications to date. For details the reader is advised to read the original papers.

12. Contrast reversal: an unsolved problem

For specimens highly inclined (i.e. tilted by 60° or more), the contrast reverses for channelling about Bragg planes perpendicular to the axis of tilt; bands usually brighter-than-background becoming darker-than-background and edges, which are usually darker, becoming brighter-than-background. This occurs when detecting back-scattered electrons, but not when detecting secondary electrons. It is independent of the detector position and is thus not a consequence of geometry. Vicario *et al.* [10] reported the effect in silicon single crystals, and the author has observed it in alkali halide and metal crystals, so it is a genuine diffraction phenomenon. In appearance, ECP contrast reversal is similar to that reported by Alam *et al.* [52] for reflection Kikuchi patterns. The origin, however, is probably different and is yet to be clearly explained.

It should be noted that contrast reversal is distinct from contrast asymmetry which is also observed when examining tilted specimens. In this case, the associated reflecting planes are inclined to the crystal surface (assuming a flat specimen) whereas in contrast reversal they are perpendicular to the surface. ECP asymmetry can be explained in terms of the electron channelling mechanism, as discussed by Booker [6] and by Spencer and Humphreys [53].

TABLE I Summary of SEM-ECP applications

Application	Material investigated	References
Standard scanning beam		
Ion implantation damage in semiconductors	Si Si GaAs Si	[28] [41] [27] [26]
Epitaxial growth	Ge on Si	[42]
Electron irradiation damage in alkali halide crystals	NaF KCl NaCl KBr	[43] [44]
Lattice parameter measurements	Si, Ge	[10] [45]
820 kV deuteron damage in silicon	Si	[45]
Detection of surface demagnetizing fields	Co	[46]
Measurement of incident beam energy in the SEM	Si	[22]
Assessment of crystal surface	GaAs Si, Al Cu, Au	[59]
Selected area		
Strain concentration in the vicinity of cracks	316 SS discaloy Ni	[19]
	304 SS 6061-T6 Al Fe–3 Si	[47]
Fracture surface analysis	Mo–Re Si	[25] [48]
Precipitate analysis	Ti (N, C)	[48]
Phase transformation	Cu–Zn Fe–Ni Martensite	[49] [21]
Superplastic deformation	Pn–Sb	[50]
Orientation relationships in martensite	Fe–Ni–C martensite	[51]

13. Comparison with other SEM methods

Other methods used to obtain crystallographic information from specimens in the SEM are the X-ray Kossel pattern technique and the electron back-scattering pattern technique [55]. The author has had no direct experience with these methods and must rely on comments by others [21, 54–56] to make the points of comparison. Before doing so, however, a few descriptive remarks are in order.

In the Kossel pattern method, the electron beam is stationary and focused on the surface of a bulk sample. The method thus utilizes an effective point-source of divergent characteristic X-rays which are diffracted from a single crystallite, thereby forming numerous diffraction and absorption conics which are recorded on film. The conics are called Kossel lines.

The electron beam is stationary in the electron back-scattering pattern (EBSP) technique [55] also. In this case the angular distribution of back-scattered electrons forms a crystallographic pattern which is almost identical to an ECP. Like Kossel patterns, EBSPs are recorded either on film or a fluorescent screen which is viewed in transmission by a closed circuit TV system.

Some points of comparison are:

(i) Both ECPs and EBSPs rely on efficient scattering processes compared with the inefficient one in the case of Kossel patterns; back-scattered coefficients are often in the range 0.1 to 0.6 compared with an efficiency of $\simeq 10^{-4}$ per electron for a characteristic X-ray. As a result, the X-ray method requires long exposures (1 to 10 min) even with relatively high beam currents ($\sim 10^{-7}$ A). EBSPs, on the other hand, require an exposure of less than 1 sec using a beam current of $\simeq 10^{-6}$ A, and ECPs may be generated using scan frame times of the order of 1 sec for a beam current around 10^{-9} A. Time-dependent phenomena such as *in situ* plastic deformation, recovery recrystallization, phase transformations, film growth, etc, are thus more readily studied using the electron scattering methods. If the specimen is susceptible to electron irradiation damage, (e.g. the alkali halides [43, 44]) then the ECP method is to be preferred.

(ii) In the electron methods, both the micrograph and the patterns can be generated simultaneously [57]. Consequently, an initial assessment can be made and only the important patterns permanently recorded. In the Kossel techniques, only "post mortems" are possible and the vacuum must be broken after each examination. This limitation has been reduced to some extent by using a ten-plate magazine [58].

(iii) The accuracy of surface orientation determinations is about the same for all three methods, $\pm 1.0°$.

(iv) The lattice parameters obtained using ECPs are accurate to 0.1%. Because of the similarity of the patterns, the precision when using EBSPs is probably the same. With the Kossel technique, on the other hand, lattice parameters can be determined to an accuracy of 0.01% [54].

(v) A consequence of (iv) is that ECPs are less sensitive to lattice strain so that mildly deformed samples give good ECPs but only poor Kossel patterns. Presumably, EBSPs are similar to ECPs in this respect.

(vi) ECP contrast arises within the first few hundred Å below the specimen surface. Kossel lines originate within the top 1 to 3 μm. The definition of Kossel patterns is thus less dependent on surface perfection.

(vii) SACPs are routinely generated from areas 5 μm diameter and from areas as small as 1 μm in diameter if electronic corrections are applied to the final lens. EBSPs are generated from regions the lateral extent of which is as small as, if not smaller than, the size of the electron cascade. Kossel patterns are obtained from surface areas as small as 5 to 10 μm diameter.

(viii) Typically, an ECP is limited to an angular width of 6 to 10° in the stereographic triangle, while EBSPs may be as wide as 60°. The wider "field of view" means that the identification of crystallographic orientation is easier.

(ix) Only materials having atomic numbers Z between 19 and 31 can be examined using the Kossel technique [56]. This limitation arises because the characteristic radiation is too long for self-diffraction for elements of $Z < 19$ and because the energy required for intense excitation of the $K\alpha$ characteristic lines in materials for which $Z > 31$ is greater than that currently available in commercial SEMs. This limitation does not apply for the ECP and EBSP methods.

14. Concluding remarks

This review has attempted to outline progress in the development of SEM electron channelling techniques since Coates first observed patterns and Booker *et al.* explained their origin, ten years ago. The optimum conditions for generating patterns and a method for obtaining them from small, selected areas of bulk materials have been established, while the detection and characterisation of crystal defects near the surface of bulk specimens are now well on the way to being realized.

Acknowledgements

The author thanks D.O. Northwood, CRNL, and S. Saimoto, Queen's University, Kingston, for comments on the manuscript.

References

1. D. G. COATES, *Phil. Mag.* **16** (1967) 1179.
2. G. R. BOOKER, A. M. B. SHAW, M. J. WHELAN and P. B. HIRSCH, *Phil. Mag.* **16** (1967) 1185.
3. P. B. HIRSCH, A. HOWIE and M. J. WHELAN, *Phil. Mag.* 7 (1962) 2095.
4. P. DUNCUMB, *Phil. Mag.* **7** (1962) 2101.
5. C. W. OATLEY, W. C. NIXON and R. F. W. PEASE, *Adv. El. and El. Phys.* **21** (1965) 181.
6. G. R. BOOKER, "Scanning Electron Microscopy" in "Modern Diffraction and Imaging Techniques in Materials Science", edited by S.A. Amelinckx, R. Gevers, G. Remant and J. Van Landuyt (North-Holland, Amsterdam, 1970) p. 553.
7. G. C. VAN ESSEN, E. M. SCHULSON and R. H. DONAGHAY, *Nature* **225** (1970) 847.

8. P. B. HIRSCH, A. HOWIE, R. B. NICHOLSON, D. W. PASHLEY and M. J. WHELAN, "Electron Microscopy of Thin Crystals", (Butterworths, London, 1965)
9. P. B. HIRSCH and C. J. HUMPHREYS, Proceedings of the Second Annual SEM Symposium (Chicago, 1969) p. 451.
10. E. VICARIO, M. PITAVAL and G. FONTAINE, *Acta Cryst.* **A27** (1971) 1.
11. J. P. SPENCER, C. J. HUMPHREYS and P. B. HIRSCH, *Phil. Mag.* **26** (1972) 193.
12. R. SANDSTROM, J. F. SPENCER, and C. J. HUMPHREYS, *J. Phys. D: Appl. Phys.* **7** (1974) 1030.
13. E. M. SCHULSON, *Phys. Stat. Sol. (b)* **46** (1971) 95.
14. E. M. SCHULSON, C. G. VAN ESSEN and D. C. JOY, Proceedings of the Second Annual SEM Symposium (Chicago, 1969) p. 45.
15. A. M. B. SHAW, G. R. BOOKER and D. G. COATES *J. Phys. E: J. Sci. Instrum.* **2** (1969) 243.
16. E. M. SCHULSON, *Rev. Sci. Instrum.* **44** (1973) 348.
17. E. M. SCHULSON and C. G. VAN ESSEN, *J. Phys. E: J. Sci. Instrum.* **2** (1969) 247.
18. E. M. SCHULSON, *J. Mater. Sci.* **6** (1971) 447.
19. R. STICKLER and G. R. BOOKER, "Electron Microscopy and Structure of Materials", edited by G. Thomas, R. Fulrath and R. Fisher (Univ. of Calif. Press, 1972) p. 301.
20. E. M. SCHULSON, *J. Phys. E: J. Sci. Instrum.* **2** (1969) 361.
21. D. C. JOY, G. R. BOOKER, E. D. FEARON and M. BEVIS, Proceedings of the Fourth Annual SEM Symposium (Chicago, 1971) p. 497.
22. E. M. SCHULSON, *J. Appl. Phys.* **42** (1971) 3894.
23. D. E. NEWBURY and D. C. JOY, Proceedings of the 25th Anniversary Meeting of EMAG (Inst. of Phys., London, 1971) p. 306.
24. C. G. VAN ESSEN, E. M. SCHULSON and R. H. DONAGHAY, *J. Mater. Sci.* **6** (1971) 213.
25. D. L. DAVIDSON, *J. Mater. Sci.* **9** (1974) 1091.
26. S. M. DAVIDSON and G. R. BOOKER, in "Ion Implantation", edited by F.H. Eisen and L.T. Chadderton (Gordon and Breach, New York, 1970) p. 51.
27. E. D. WOLF and R. G. HUNSPERGER, Proceedings of the Third Annual SEM Symposium (Chicago, 1970) p. 457.
28. E. M. SCHULSON and D. A. MARSDEN, *Rad. Effects* **24** (1975) 195.
29. D. R. CLARKE, *Phil. Mag.* **24** (1971) 973.
30. R. M. STERN, T. ICHINIKAWA, S. TAKASHIMA, H. HASHIMOTO and S. KIMOTO, *Phil. Mag.* **26** (1972) 1495.
31. G. R. BOOKER, D. C. JOY, J. P. SPENCER and C. J. HUMPHREYS, Proceedings of the Sixth Annual SEM Symposium (Chicago, 1973) p. 252.
32. D. R. CLARKE, and A. HOWIE, *Phil. Mag.* **24** (1971) 959.
33. C. J. HUMPHREYS, J. P. SPENCER, R. J. WOOLF, D. C. JOY, J. M. TITCHMARSCH and G. R. BOOKER Proceedings of the Fifth Annual SEM Symposium (Chicago, 1972) p. 205.
34. A. V. CREWE and J. WALL, *J. Mol. Biol.* **48** (1970) 375.
35. "Electron Microscopy 1972", Proceedings of the Fifth European Congress on Electron Microscopy Manchester (Inst. of Physics, London, 1972).
36. "Electron Microscopy 1974", Proceedings of the Eighth International Congress on Electric Microscopy, Canberra 1974 (Australia Aca. Sci., Canberra)
37. C. G. VAN ESSEN, Proceedings of the 25th Anniversary Meeting of EMAG, (Inst. of Phys., London, 1971) p. 314.
38. D. C. JOY, and D. E. NEWBURY, *J. Mater. Sci.* **7** (1972) 714.
39. G. R. BOOKER and R. STICKLER, Proceedings of the Fifth Annual SEM Symposium (Chicago, 1972) p. 225.
40. *Idem, J. Mater. Sci.* **7** (1972) 712.
41. S. M. DAVIDSON, *J. Mater. Sci.* **7** (1972) 473.
42. P. DURUPT, A. LAUGIER, M. PITAVAL and E. VICARIO, *Compt. Rend.* **270B** (1970) 941.
43. E. M. SCHULSON, *J. Mater. Sci.* **6** (1971) 377.
44. *Idem,* Proceedings of the Fourth Annual SEM Symposium (Chicago, 1971) p. 489.
45. E. VICARIO, Ph.D. Thesis University of Lyon, (1970).
46. D. C. JOY, E. M. SCHULSON, J. P. JAKUBOVICS and C. G. VAN ESSEN, *Phil. Mag.* **20** (1969) 843.
47. D. L. DAVIDSON and J. LANGFORD JUN., *J. Eng. Mater. & Tech.* (TASME) paper no. 75-MAT-6 (1975).
48. G. R. BOOKER, D. C. JOY and R. STICKLER, Proceedings of the 25th Anniversary of EMAG (Inst. of Phys., London, 1971) p. 294.
49. J. D. AYERS and D. C. JOY, *Acta Met.* **20** (1972) 1371.
50. D. C. JOY and D. E. NEWBURY, *J. Mater. Sci.* **7** (1972) 113.
51. T. N. DURLU, "Scanning Electron Microscopy; Systems and Applications, 1973" (Inst. of Phys., London, 1973) p. 320.
52. M. N. ALAM, M. BLACKMAN and D. M. PASHLEY *Proc. Roy. Soc.* **A221** (1954) 224.
53. J. P. SPENCER and C. J. HUMPHREYS, Proceedings of the 25th Anniversary Meeting of EMAG (Inst. of Phys., London, 1971) p. 310.
54. R. E. HANNEMAN, R. E. OGILVIE and A. MODRZEJEWSKI, *J. Appl. Phys.* **33** (1962) 1429.
55. J. A. VENABLES and C. J. HARLAND, *Phil. Mag.* **27** (1973) 1193.
56. D. J. DINGLEY and S. BIGGIN, "Scanning Electron Microscopy: Systems and Applications, 1973" (Inst. of Phys., London, 1973) p. 308.
57. D. C. JOY and G. R. BOOKER, Proceedings of the 25th Anniversary Meeting of EMAG (Inst. of Phys. London, 1971) p. 316; *J. Phys. E: J. Phys. Instrum.* **4** (1971) 837.
58. D. J. DINGLEY and S. BIGGIN, "Scanning Electron Microscopy: Systems and Applications, 1973" (Inst. of Phys., London, 1973) p. 314.
59. E. M. SCHULSON, Report of the Atomic Energy of Canada Ltd. (1971) 4069.

Received 28 August and accepted 4 October 1976.